DAMAGE EVOLUTION BY ACOUSTIC EMISSION METHOD IN THE FRACTURE PROCESS ZONE OF CONCRETE

(Translation from Proceedings of JSCE, No. 599/V-40, August 1998)

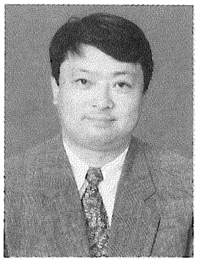

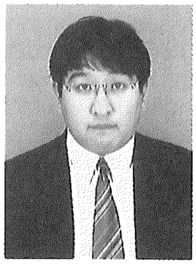

Masayasu OHTSU   Masanobu OHTSUKA

The moment tensor analysis of acoustic emission (AE) is reviewed from the standpoint damage mechanics. The relationship between the damage variable and the moment tensor is clarified. In bending tests on notched beams, the crack kinematics are determined: tensile cracks nucleate extensively in the outer regions of the fracture process zone, while shear cracks are observed within the zone and close to the final crack surface. The damage evolution process during nucleation of the fracture process zone is estimated. It is found that the evolution process in cementitious materials is not necessarily dependent on the mode of final cracking, but is associated closely with the mechanism of microcracking.

Keywords : acoustic emission, moment tensor analysis, fracture process zone, damage mechanics

---

Masayasu Ohtsu is a Professor in the Department of Civil Engineering and Architecture, Kumamoto University, Kumamoto, Japan. He obtained Dr. Eng. from Kyoto University in 1983. He has been studying extensively applications of AE and related NDE techniques for structures. He is a member of JSCE and currently a chairman of the research subcommittee on Diagnosis for Structures.

Masanobu Ohtsuka is a research engineer at Oriental Construction Corp., Fukuoka, Japan. He obtained Ms. Eng. from Kumamoto University in 1997. His research covers diagnostic applications of AE to concrete structures. He is a member of JSCE.

---

1. INTRODUCTION

Acoustic emission (AE) is an inspection technique in which elastic waves generated in a material are detected. It has been confirmed that in concrete AE waves due to cracking can be synthesized by the dislocation mode[1]. Dislocation (crack) motion consists of kinetics and kinematics. In source characterization of AE, crack kinetics is represented by a source-time function which can be determined by deconvolution analysis[2]. Crack kinematics at the AE source is defined by the crack motion vector (Burgers vector) and the unit vector normal to the crack plane. Combined with the elastic constants, the product of the two vectors leads to the moment tensor. A simplified and stable procedure has been developed to determine moment tensor components from AE waveforms[3]. Based on an eigenvalue analysis of the moment tensor, a generalized treatment for the classification of crack type and the determination of crack orientation is now implemented as the SiGMA (simplified Green's functions for moment tensor analysis) code[4]. The procedure has been successfully applied to fracture tests of concrete[5],[6],[7]. Elsewhere, a similar procedure has been reported[8] but is limited to the two-dimensional (2-D) problem, for which the SiGMA-2D code is available[9].

In order to apply fracture mechanics to the fracture modes of concrete structures, the nucleation of the fracture process zone ahead of the crack tip has been intensively studied[10]. Recently, also fracture mechanics has been extended to cover continuous damage mechanics[11]. In this paper, the relation between the damage variables and the moment tensor components is clarified. In bending tests on notched beams, crack kinematics and damage evolution in the fracture process zone are estimated by moment tensor analysis using SiGMA.

2. MOMENT TENSOR AND DAMAGE VARIABLES

Mathematically, crack kinematics can be modeled using crack motion vector $\mathbf{b}(\mathbf{y},t)$ and the unit vector $\mathbf{n}$ normal to crack surface F, as shown in Fig. 1. Vector $\mathbf{b}(\mathbf{y},t)$ is referred to as $b(\mathbf{y})\mathbf{l}S(t)$, where $b(\mathbf{y})$ represents the magnitude of crack displacement, $\mathbf{l}$ is the direction vector of crack motion, and $S(t)$ is the source-time function of crack nucleation. The following integration over crack surface F leads to a product of the moment tensor m_{pq} and the source-time function $S(t)$:

$$\int_F C_{pqkl}\,[b(\mathbf{y})l_k S(t)]\,n_l\,dS = [C_{pqkl}\,l_k n_l]\,[\int_F b(\mathbf{y})\,dS]S(t)$$

$$= [C_{pqkl}\,l_k n_l]\,\Delta V\,S(t) = m_{pq}\,S(t), \qquad (1)$$

where C_{pqkl} is the tensor of elastic constants and ΔV is the crack volume.

The elastic displacement $\mathbf{u}(\mathbf{x},t)$ due to crack motion $\mathbf{b}(\mathbf{y},t)$ represents AE wave[3],

$$u_i(\mathbf{x},t) = G_{ip,q}(\mathbf{x},\mathbf{y},t)\,m_{pq} * S(t). \qquad (2)$$

Here $G_{ip,q}(\mathbf{x},\mathbf{y},t)$ are the spatial derivatives of Green's functions and the symbol $*$ denotes the convolution operation.

In an isotropic material, the moment tensor m_{pq} is derived from eq. (1),

$$m_{pq} = [C_{pqkl}\,l_k n_l]\,\Delta V = [\lambda l_k n_k + \mu l_p n_q + \mu l_q n_p]\Delta V, \qquad (3)$$

where λ and μ are Lame constants. The product of crack vector $b(\mathbf{y})l_k$ and crack normal n_l is referred to in micromechanics as the eigenstrain [12]. Similarly, in damage mechanics, the second-order damage tensor εP_{kl} is defined[13] as,

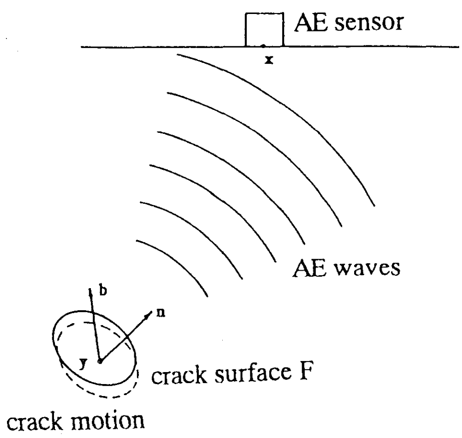

Fig. 1 Crack nucleation and AE waves.

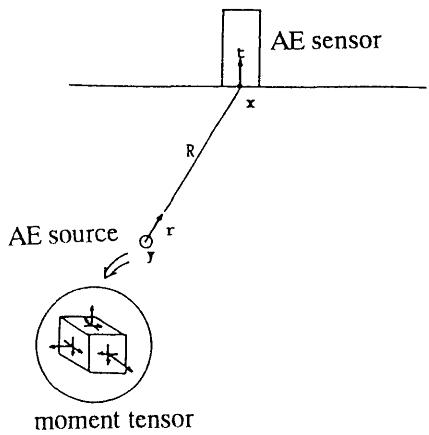

Fig. 2 Configuration of AE sensors and AE source.

$$\varepsilon P_{kl} = 1/V^* \sum_i \Delta F \, (b_k n_l + b_l n_k)^{(i)} / 2, \tag{4}$$

where V* is the representative volume and ΔF is the area of one crack. Taking into account only one crack, the damage tensor $\varepsilon 1_{kl}$ for one crack is derived from eq. (4),

$$\varepsilon 1_{kl} = 1/V^* \int_F ([b(\mathbf{y})l_k]\, n_l + [b(\mathbf{y})l_l]\, n_k) dS / 2 = \Delta V \, (l_k n_l + l_l n_k) / 2V^*. \tag{5}$$

The scalar damage variable for one crack D is readily obtained as,

$$D = n_k \, \varepsilon 1_{kl} \, n_l = \Delta V / V^* \, l_k n_k. \tag{6}$$

From eq. (3), a trace component is obtained,

$$m_{kk} = (3\lambda + 2\mu) \, l_k n_k \Delta V. \tag{7}$$

Consequently, the damage evolution can be represented as,

$$\sum_i D^{(i)} = 1 / V^* \sum_i [\Delta V \, l_k n_k]^{(i)} = 1 / [V^* (3\lambda + 2\mu)] \sum_i m_{kk}{}^{(i)}. \tag{8}$$

This implies that the damage evolution process can be estimated in relative terms from the accumulation of trace components of the moment tensors. Also, the relative crack volume can be obtained from eq. (7) as,

$$(3\lambda + 2\mu) \, \Delta V = m_{kk} / [l_k n_k]. \tag{9}$$

3. SiGMA PROCEDURE

In the SiGMA code, eq. (2) is simplified, taking into account only the amplitude of first motion A(**x**) of AE wavefrom in the far field,

$$A(\mathbf{x}) = Cs / R \; Ref(\mathbf{t}, \mathbf{r}) \, r_p \, m_{pq} \, r_q, \tag{10}$$

where Cs is the calibration coefficient. As shown in Fig. 2, **t** is the direction of sensor sensitivity.

R is the distance from the AE source at point $\mathbf{y}$ to the AE sensor at point $\mathbf{x}$. r_p is its direction vector. $Ref(\mathbf{t},\mathbf{r})$ is the reflection coefficient. Since the moment tensor is symmetric and of the second order, the number of independent unknowns m_{pq} is six. A multi-channel observation of first motions at more than six sensor locations can provide sufficient information to solve eq. (10).

Prior to the analysis, the calibration coefficient Cs in eq. (10) should be determined to compensate for the sensitivity of the AE sensors. Three eigenvalues are then normalized and uniquely decomposed into three ratios X, Y, and Z[4],

$$\begin{aligned}
&1.0 = X + Y + Z, \\
&\text{the intermediate eigenvalue/the maximum} \\
&\qquad = 0 - Y/2 + Z, \\
&\text{the minimum eigenvalue/the maximum} \\
&\qquad = - X - Y/2 + Z,
\end{aligned} \tag{11}$$

where X, Y, and Z denote the shear ratio, the deviatoric tensile ratio, and the isotropic tensile ratio, respectively. AE sources for which the shear ratios X are smaller than 40% are classified as tensile cracks. AE sources of the shear ratio X greater than 60% are referred to as shear cracks. In cases between 40% and 60%, the AE source is classified as mixed-mode.

In the SiGMA code, unit vectors $\mathbf{e}_1$, $\mathbf{e}_2$ and $\mathbf{e}_3$ corresponding to the three eigenvectors $\mathbf{l} + \mathbf{n}$, $\mathbf{l} \times \mathbf{n}$, and $\mathbf{l} - \mathbf{n}$ are determined. Therefore, vectors $\mathbf{l}$ and $\mathbf{n}$ can be recovered from the following relations,

$$\begin{aligned}
\mathbf{l} &= (2 + 2l_k n_k)^{1/2}\mathbf{e}_1 + (2 - 2l_k n_k)^{1/2}\mathbf{e}_3, \\
\mathbf{n} &= (2 + 2l_k n_k)^{1/2}\mathbf{e}_1 - (2 - 2l_k n_k)^{1/2}\mathbf{e}_3.
\end{aligned} \tag{12}$$

4. EXPERIMENTS

4.1 Bending Tests

The flaw location procedure was successfully applied to identify the fracture process zone in concrete[14]. Because the SiGMA procedure provides information on crack types and crack orientation, in addition to crack location, crack nucleation in the fracture process zone is investigated.

Mortar and concrete specimens of dimensions 10 cm x 10 cm x 40 cm were cast and cured in water for 28 days in a standard room (20°C). Mixture proportions are given in Table 1. The maximum size of coarse aggregate is 20 mm, and the fine aggregate is common to both of concrete and mortar mixes. Mechanical properties are indicated in Table 2. These were determined from cylindrical specimens of 10 cm in diameter and 20 cm in height at the age of 28 days. Although the strength of mortar is comparable to that of concrete, Young's modulus and P-wave velocity of mortar are lower than those of concrete.

Three-point bending tests were conducted. At the age of 28 days, a sawed pre-cracked notch of 3 cm depth and 1 mm width was introduced in each specimen. The types of specimen included a center-notched beam under center loading (type CC), and an off-center notched beam under center loading (type OC). The experimental set-ups and AE sensor locations are shown in Fig. 3. Six AE sensors were arranged to cover the area of the fracture process zone to be nucleated. In the figures, open circles indicate AE sensors located on the back face and solid circles those on the front face. All sensors have a resonant frequency of 150 kHz. They were relatively calibrated so as to obtain equivalent sensitivities beforehand. The measured frequency was 10 kHz - 1 MHz and a total 60 dB gain for amplification was employed.

AE waveforms occurred during crack extension were detected, amplified, filtered, and recorded using the LOCAN-TRA system (Physical Acoustics Corp.). Loads were measured with a loadcell

Table 1 Mixture proportions

	weight per unit mass (kg/m³)				(cc)	(cm)	(%)
	W	C	S	G	AE admix-ture	slump	air
concrete	172	346	834	1021	104	8.0	5.0
mortar	342	570	1140	-	-	-	-

Table 2 Mechanical properties

	compre-ssive strength (MPa)	tensile strength (MPa)	Poi-sson's Ratio	Young's modulus (GPa)	P-wave velocity (m/s)
concrete	52.8	4.12	0.24	32.5	4730
mortar	53.7	2.93	0.20	23.4	4130

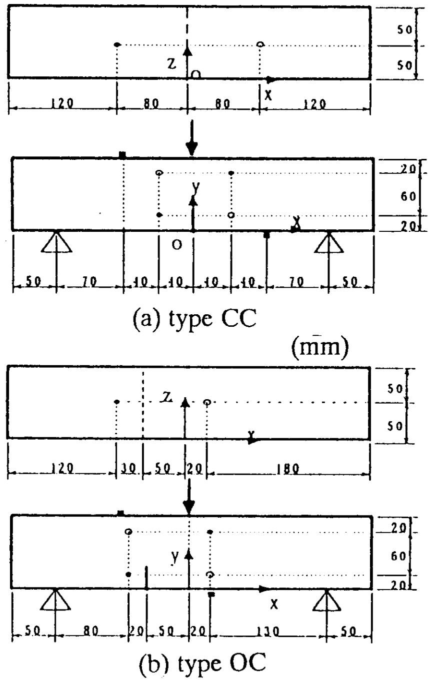

Fig. 3 Experimental set-up and AE sensor array.

and crack-mouth opening displacements (CMOD) were recorded using a clip gauge inserted into the notch. A servo-valve controlled machine was employed for loading.

Specimens of type CC were prepared to trace the nucleation of the fracture process zone under mode-I cracking. In contrast, mixed-mode of mode-I and mode-II cracking was expected in type OC. Loading rate of 0.01 mm/min was applied to type CC specimens, whereas the rate applied to type OC specimens was 0.02 mm/min. This is because crack propagation in type CC was faster than that in type OC.

4.2 Waveform Analysis

In order to solve eq. (10), the amplitude of the first motion should be read from AE waveform. In addition, the arrival time of the first motion needs to be determined to carry out location analysis. These two parameters of the arrival time and the amplitude of the first motion were read visually from each waveform as displayed on the CRT screen. From the AE waveforms at six locations, the locations and moment tensor components were determined. The crack types and crack orientations were then analyzed.

In order to estimate errors in the moment tensors, error analysis was performed with assumed location errors[4]. As a result, it was realized that accuracy was highly dependent on the geometrical configuration of the sensor array and the AE sources. This in turn implies that the solution accuracy is dependent on particular situation and may not be estimable by simple criteria. Furthermore, it was found that most errors were introduced by misreading the first motions. To select reliable solutions, therefore, a method of post-analysis was developed[15]. Theoretical AE waveforms at the AE sensor locations were synthesized, using data on the AE source location and the moment tensor components. The two parameters of each theoretical waveform were automatically read and the SiGMA code was applied again. Then, AE sources whose crack kinematics in post analysis were in good agreement with those of the SiGMA analysis were selected as reliable solutions.

Table 3 The number of AE hits analyzed

		total AE hits	clear records	SiGMA analyzed	post-analysis
concrete	type CC	205	177	137	36
	type OC	515	212	143	29
mortar	type CC	254	207	147	43
	type OC	975	609	409	102

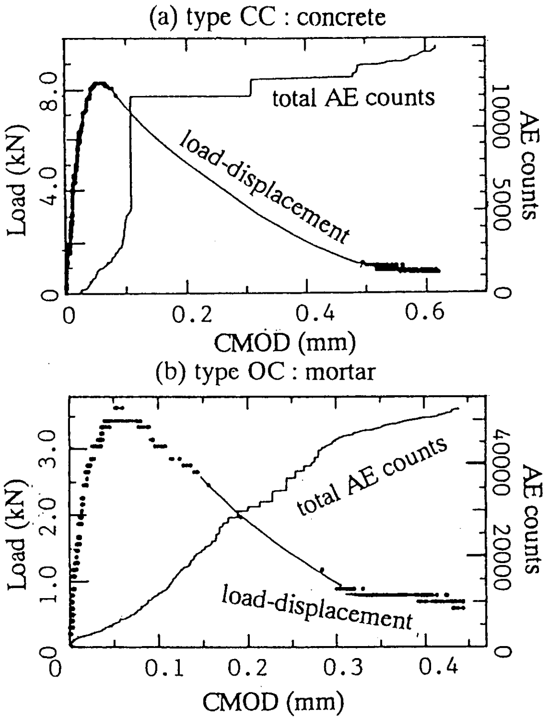

Fig. 4 Load-CMOD relations and Total AE counts observed under loading.

5. RESULTS AND DISCUSSION

The number of total AE hits detected in the tests is indicated in Table 3. An AE hit is defined as an AE event for which AE waveforms are simultaneously recorded on all channels. Among this AE hit data, however, not all first motions could necessarily be identified. Thus AE hits for which first motions were clearly recorded on all six channels were selected for analysis. The number of these data is denoted in the table. In the case of concrete type OC, more than 50% of AE hits were discarded. After SiGMA analysis, approximately half of the total AE hits reached solution except for concrete type OC. Eventually, in post-analysis, the number of data points further decreases to 10 - 20% of the total. This is a limitation of the feasibility of SiGMA analysis in its current state. AE events discarded in the analysis mostly result from unclear first motions and divergence in the location routine. The situation might be improved by introducing automated first-motion reading[8].

In contrast to AE hits, AE counts are defined as the number of AE occurrences recorded on one channel. In Fig. 4, AE counts observed by the AE sensor on channel 1 are plotted against CMOD, along with the load-displacement curve. Concrete type CC, as shown in Fig. 4 (a), is a typical result. After the peak load, AE activity suddenly increases and thus discontinuous jumps in AE occurrence are observed. In concrete type OC, similar activity was found. This suggests that the cracking process in concrete is not continuous. As shown in Fig. 4 (b), in the case of mortar type OC, AE activity increases gradually with no relation to peak load. Although a slight increase in AE activity was seen at peak load in mortar type CC, the essential behavior of AE occurrence is similar to Fig. 4 (b). This implies that microcracks in the fracture process zone are generated continuously in mortar.

The results of post analysis are plotted in Figs. 5 and 6. AE sources for which the shear ratios are smaller than 40%, and are therefore classified as tensile cracks, are indicated by the "arrow" (⇔) symbol, while other sources are indicated by the "cross" (×) symbol.

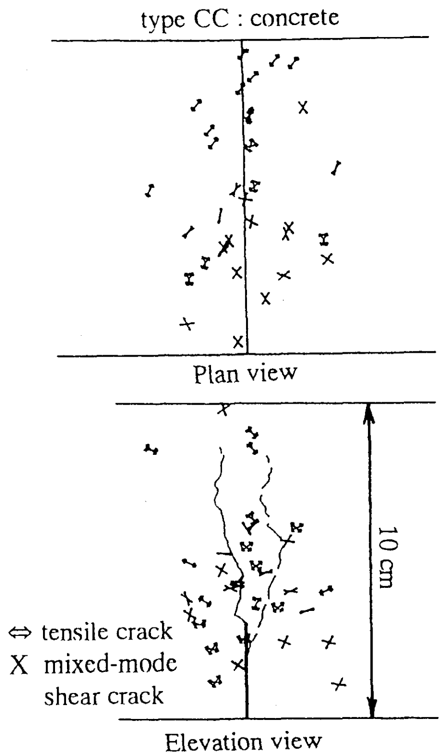

Fig. 5 Crack locations, types and orientations determined in a concrete specimen of type CC.

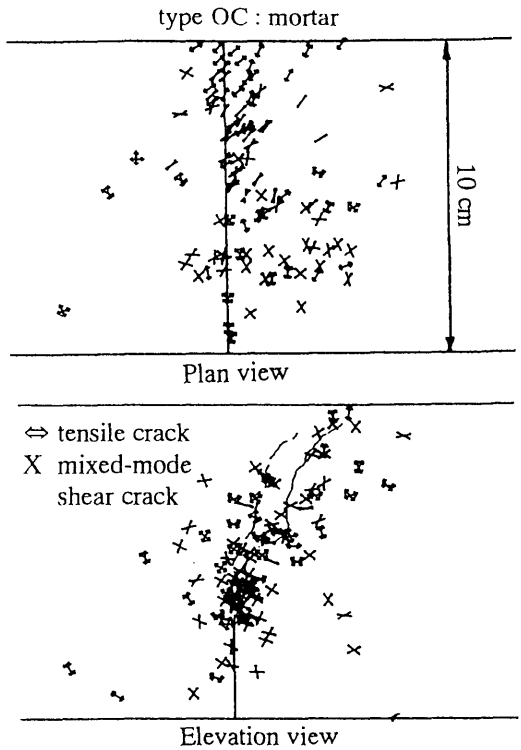

Fig. 6 Crack locations, types and orientations determined in a mortar specimen of type OC.

AE sources are plotted at their locations with directing the two vectors **l** and **n**, which are determined from eq. (12). Previously, only the first eigenvectors $\mathbf{e}_1$ were plotted for tensile cracks[4]. A recent study, however, clarifies that the angle between the two vectors **l** and **n** could be over 50°, even in a case where the shear ratio is smaller than 40%[16]. Consequently, the directions of the two vectors are given for all data. Naturally, the angle between the two vectors is considerably smaller for tensile cracks with the "arrow" symbol.

In Fig. 5, the result for a concrete specimen of type CC is given. Surface cracks extending from the notch are indicated in the elevation view. These were observed at the front face and the back face. The final crack surface follows a tortuous path to the notch, and thus the direction of the tensile opening is inclined toward the notch according to the plan view. It seems that an AE cluster covers the fracture process zone and tensile cracks are observed in the outer regions of the zone.

In Fig. 6, the result for a mortar specimen of type OC is shown. Surface cracks form diagonally from the notch to the loading point. Thus, mixed-mode crack propagation is observed. Along the final crack surface, there is an intense AE cluster. Under mixed-mode cracking, a wide region corresponding to the fracture process zone is observed. Again, tensile cracks are mainly observed far from the surface cracks and the cluster of shear cracks.

To confirm the apparent trend in AE location, AE sources are projected onto the x-y plane in Fig. 3. The case of a concrete specimen of type OC is shown in Fig. 7. Cracks are classified into tensile, mixed-mode, and shear cracks. The locations of surface cracks are denoted by open circles. The

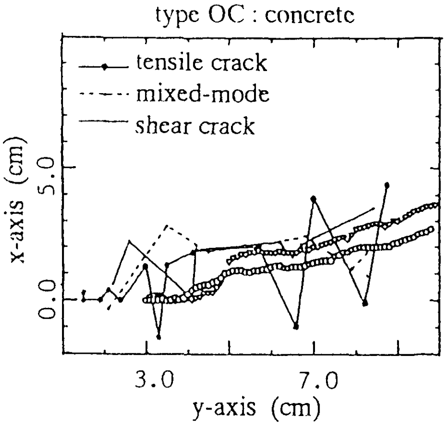

Fig. 7 Projection of AE locations in concrete type OC.

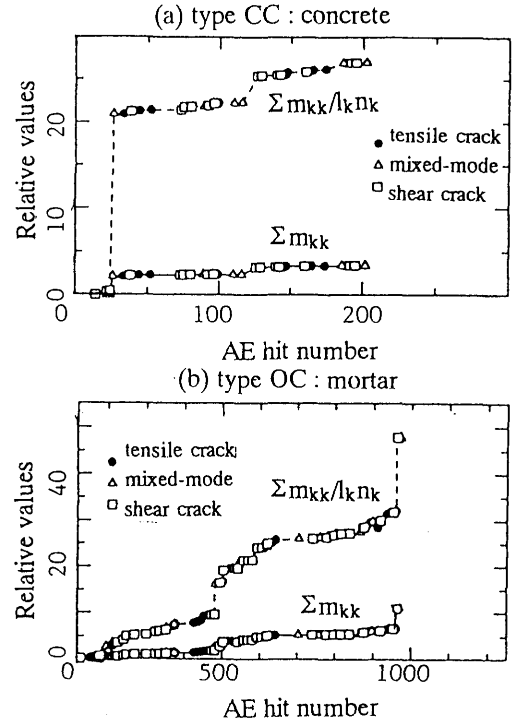

Fig. 8 Damage evolution and the accumulation of crack volume.

final crack extends from left to right. Most of the tensile cracks are observed further from the surface cracks than mixed-mode and shear cracks, which are observed close to the surface cracks. Similar results were also obtained in the other cases. This demonstrates that tensile cracks nucleate in the outer regions of the fracture process zone, while other types of cracks are generated intensely within the process zone.

Damage evolution was estimated using eq. (8). The accumulation of crack volume was also estimated from eq. (9). In Fig. 8, results for concrete type CC and mortar type OC are plotted. The trace of the moment tensor was directly calculated from the experimental results. Consequently both the scalar damage m_{kk} and the variable $m_{kk}/l_k n_k$ corresponding to the crack volume are relative. The accumulation of these values is plotted against the number of AE hits. Although the cracks are categorized, three types of cracks are generated in so much confusion that the dominant type cannot be identified in the accumulation process. As seen in Fig. 8 (a), damage evolution and the accumulation of crack volume rise discontinuously. According to Fig. 8 (b), the damage evolution in mortar is fairly continuous although a slight step increase is observed in the accumulation of crack volume.

Taking into account the difference in AE activity shown in Fig. 4, the discrepancy in damage evolution might result from the presence of the coarse aggregate in concrete specimens. The step-like increases in damage and crack volume possibly correspond to bonding failures between coarse aggregate and the mortar matrix.

In type CC specimens, mode I cracking was expected, while mixed-mode cracking was suggested in type OC. This difference in damage evolution process was, however, not clear in concrete. The evolution process was always step-like discontinuous. On the other hand, damage evolution of mortar was observed to be continuous as nucleation of the fracture process zone proceeded. This implies that damage evolution in the fracture process zone of cementitious materials is not necessarily dependent on the final crack mode, but is responsible for the nucleation of microcracking.

6. CONCLUSION

By applying moment tensor analysis to AE, the damage evolution process during nucleation of the fracture process zone is estimated in concrete and mortar. The conclusions reached are as follows:

(1) Although specimens were prepared for mode-I cracking and for mixed-mode cracking, the cracking process (AE generation) in both cases is observed to be not continuous in concrete. In contrast, microcracks are generated continuously in the fracture process zone of mortar.

(2) From SiGMA analysis, it is found that tensile cracks appear further from the surface cracks than mixed-mode and shear cracks. This demonstrates that tensile cracks nucleate in the outer regions of the fracture process zone, while shear cracks are generated within the zone and close to the final crack surface.

(3) In concrete, damage evolution in the fracture process zone is step-like discontinuous, while in mortar it is almost continuous. The difference between mode-I cracking and mixed-mode cracking in the damage evolution process is not clear. This implies that damage evolution in cementitious materials is not necessarily dependent on the mode of final cracking, but is rather associated closely with the nucleating mechanism of microcracking.

References

[1] Ohtsu, M.: Source Mechanism and Waveform Analysis of Acoustic Emission in Concrete, Journal of AE, Vol. 2, No. 1, 103 - 112, 1982
[2] Wadley, H. N. G., and Scruby, C. B. : Acoustic Emission Source Characterization, Advances in Acoustic Emission, Dunhart Publishers, Knoxville, 125-153, 1981
[3] Ohtsu, M.: Mathematical Theory of Acoustic Emission and Moment Tensor Solution, Journal of the Society of Materials Science, Japan, Vol. 36, No. 408, 1025-1031, 1987
[4] Ohtsu, M.: Simplified Moment Tensor Analysis and Unified Decomposition of AE Source, Journal of Geophysical Research, Vol. 96, No. B4, 6211-6221, 1991
[5] Ohtsu, M., Shigeishi, M., and Iwase, H.: AE Observation in the Pull-Out Process of Shallow Hook Anchors, Proc. JSCE, No. 408/V-11, 177-186, 1989
[6] Suaris, W. and van Mier, J. G. M.: Acoustic Emission Source Characterization in Concrete under Biaxial Loading, Materials and Structures, No. 28, 444-449, 1995
[7] Yuyama, S., Okamoto, T., Shigeishi, M., and Ohtsu, M.: Acoustic Emission Generated in Corners of Reinforced Concrete Rigid Frame under Cyclic Loading, Materials Evaluation, Vol. 53, No. 3, 409-412, 1995
[8] Ouyang, C., Landis, E., and Shah, S. P.: Damage Assessment in Concrete using Quantitative Acoustic Emission, Journal of Engineering Mechanics, ASCE, Vol. 117, No. 11, 2681-2698, 1991
[9] Shigeishi, M. and Ohtsu, M.: Acoustic Emission Waveform Analysis in Two-Dimensional Models, Journal of the Society of Materials Science, Japan, Vol. 45, No. 9, 1055-1060, 1996
[10] Mihashi, H.: State-of-the-Art Report on Fracture Mechanics Applied to Reinforced Concrete Structures, Concrete Journal, JCI, Vol. 34, No. 5, 5-15, 1996
[11] Shah, S. P., Swartz, S., and Ouyang, C. S.: Fracture Mechanics of Concrete, John Wiley & Sons, Inc., New York, 1995
[12] Mura, T.: Micromechanics of Defects in Solids, Martinus Nijhoff Publishers, The Hague, 1982
[13] Kachanov, M.: Effective Elastic Properties of Cracked Solids : Critical Review of Some Basic Concepts, Applied Mechanics Reviews, Vol. 45, No. 8, 304-335, 1992
[14] Nomura, N., Mihashi, H., and Niiseki, S.: Influence of Coarse Aggregate Size on Fracture Energy and Tension Softening of Concrete, Concrete Research and Technology, JCI, Vol. 2, No. 1, 57-66, 1991
[15] Ohtsu, M.: Post-Analysis of SiGMA Code for Acoustic Emission Moment Tensor Analysis, Journal of JSNDI, Vol. 43, No. 12, 776-782, 1994
[16] Ohtsu, M.: Acoustic Emission Theory for Moment Tensor Analysis, Research on Nondestructive Evaluation, No. 6, 169-184, 1995